Proceedings of the 2018 IEEE/ASME International Conference on Advanced Intelligent Mechatronics (AIM), Auckland, New Zealand, July 9-12, 2018



# Modeling and Analysis of Flexure-based Nano-Positioning Device Driven by Voice Coil Actuator

Xiaolu Huang[1,2], Bao Yang[1,2], Chi Zhang[2]*, Silu Chen[2], Jinhua Chen[2] and Youyong Liao[2]

***Abstract*—This paper proposes a flexure-based nano-positioning device which can yield ±2mm motion range with nearly linear relationship between input current and output displacement. The voice coil actuator (VCA) applies Halbach permanent magnet array whose thrust and force ripple are accurately modeled based on gap magnetic field analysis. The thrust model is verified by Finite Element Analysis (FEA) and VCA parameters are optimized by Genetic Algorithm (GA). The VCA coil skeleton with three coils is supported by flexure-based membranes. The membrane consists of bend segments and torsion segments which are connected in "S" shape. Equivalent models are applied to predict the stiffness of the membrane. At last, the force-displacement curve of VCA and displacement-force curve of the flexure-based membrane are obtained by experiments. The results validate the correctness of the developed model and the feasibility of the design.**

## I. INTRODUCTION

Precision actuators supported by flexure-based bearings are often implemented to realize nanometric precision. The flexure-based bearing serves as guidance with many advantages such as no backlash, no friction, no contamination and nearly free of maintenance. Many researchers use piezoelectric transducer[1] (PZT) to drive flexure-based bearing. However, the stroke of PZT is limited in hundreds micrometers. Furthermore, creep and hysteresis characteristics of PZT will cause control difficulties and decrease precision. Nowadays, realization of large motion range (>1 mm) along with nanometric motion quality (<10 nm) simultaneously[2] is the key challenge of nano-technology. Utilization of VCA as the driver is one way to overcome the stroke limitation. The flexure-based electromagnetic linear actuator[3-4] (FELA) is a good example of VCA application, it could achieve millimeters stroke in nanometric resolution. Based on FELA, a novel VCA structure was proposed in our previous work[5]. This novel VCA applies quasi-Halbach array instead of common monolithic permanent magnet (PM), and the single coil is replaced by three coils correspondingly. The test results show that quasi-Halbach array structure can improve the thrust. However, the accurate models of the thrust and force ripple were not developed and the parameters of the VCA were not optimized in that work.

Halbach array is a special arrangement of permanent magnets, with continuous different magnetization directions. In practical application, the directions are discrete, usually there are four directions i.e. 0°, 90°, 180° and -90° which are presented in Fig. 1, it is called quasi-Halbach array. It can enhance the flux density in one side (active side) and decrease the flux density in the other side (quiet side), which yields the characteristic of "self-shielding"[6-7]. Halbach arrays could be applied on PM motors to enhance the flux density and reduce force ripple, or cancel iron core so that the actuator mass will be reduced a lot[8-10]. It can also be used in magnetic bearings and magnetic gears[11]. To guarantee nice performance, the dimension parameters of the array should be carefully designed.

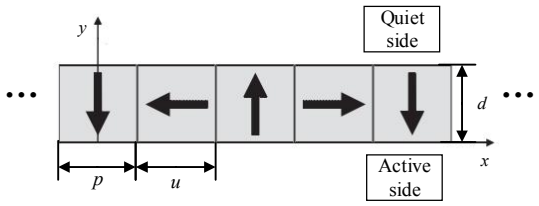



Figure 1. Quasi-Halbach array

The parametric sensitivity analysis method[3,11] can be applied in parameters optimization of the Halbach array. However, parametric sensitivity analysis is good at demonstrating the influence of parameters but inconvenient to find the optimal parameters without mathematic model. The equivalent magnetic circuit method[4,12] can model the average air gap flux density and derive the average thrust model, but the thrust will drop with coil displacement which is called force ripple or force-stroke nonlinearity[14], the average thrust model cannot depict it. The force ripple will cause hysteresis effects[13] and thereby the linear feedback is hard to compensate[14] them. Therefore, an accurate model is required to depict the force ripple.

The flexure-based bearing prefers to be designed with high stiffness to rise resonance frequency, but this requires high driving force. It should be guaranteed that the VCA can push flexure-based bearing to several millimeters. To achieve this, the thrust of VCA should be optimized as mentioned before and flexure-based bearing should be designed with low stiffness along working direction while keep high off-axis stiffness.

*Research supported by NSFC-Zhejiang Joint Fund for the Integration of Industrialization and Informatization (U1609206), the Zhejiang Basic Public Welfare Research Project (LGG18E070007) and Major Project and Key S&T Program of Ningbo (2017B10014).

[1]University of Chinese Academy of Sciences, Ningbo Institute of Materials Technology & Engineering, CAS, Ningbo 315201, China.

[2]Ningbo Institute of Materials Technology & Engineering, CAS, Zhejiang Key Laboratory of Robotics and Intelligent Manufacturing Equipment Technology, Ningbo 315201, China, (corresponding author to provide e-mail: zhangchi@nimte.ac.cn).

In this paper, magnetic field analysis method is applied to accurately depict the gap flux density distribution and develop the accurate thrust model. The thrust model is verified by FEA via ANSYS MAXWELL. Genetic algorithm is implemented to optimize the thrust and force ripple when the volume of the VCA is fixed. Flexure-based membrane is designed with beam segments connected in "S" shape. It can avoid nonlinear large deformation by accumulating small deformations. Its stiffness is predicted by equivalence principle[15-16] and the stiffness of membrane is verified via ANSYS. Low stiffness reduces the requirement of output force in VCA, but this causes the problem of low natural resonance frequency which will bring problems of vibrations and disturbs. These problems can be resolved by build-in electromagnetic damping of the VCA which will be studied in future.

## II. Modeling and Analysis of the Nano-Positioning Device

The nano-positioning device is presented in Fig. 2, two membranes deploy at both side of VCA, they comprise double parallelogram flexure mechanism, the coil skeleton is supported by the membranes and delivers a reciprocating motion. There are three coils winded on the coil skeleton, the magnetic field is excited by PMs which distinguished by four different colors. The input current is controlled to produce an expected driving force. Due to the obvious symmetry, half of the VCA is studied. In PART A, a primary simulation analysis is presented, in PART B, the accurate model is developed and in PART C, the flexure-based membrane is designed and the equivalent stiffness model is presented.

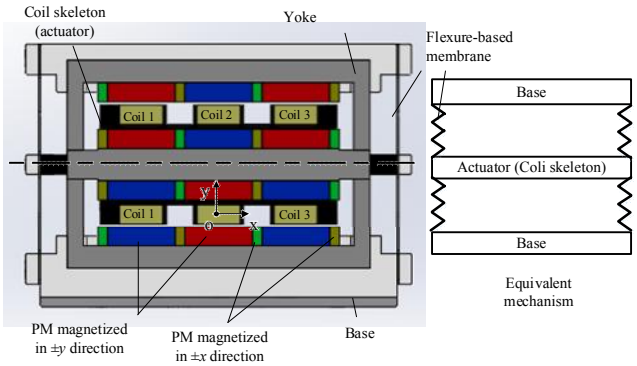



Figure 2. Profile map of the nano-positioning device and equivalent mechanism comprised of flexure-base membranes.

### A. Simulation of three different structures.

Three different structures is presented in Fig. 3, they are referred to the common structure, the segmented structure and Halbach structure respectively. Four colors, i.e., blue, red, green and yellow, represent PMs magnetized in four different directions. For Halbach structure (Fig. 3-c), if the width of narrow PMs (green and yellow) shrink to zero, it becomes to the segmented structure (Fig. 3-b). All the three structures were simulated by ANSYS MAXWELL, respectively. Current were in vertical paper direction, as shown in Fig.3 and the moving direction is horizontal. Flux line with flux density are plotted, for clarity, only yoke flux density is plotted.

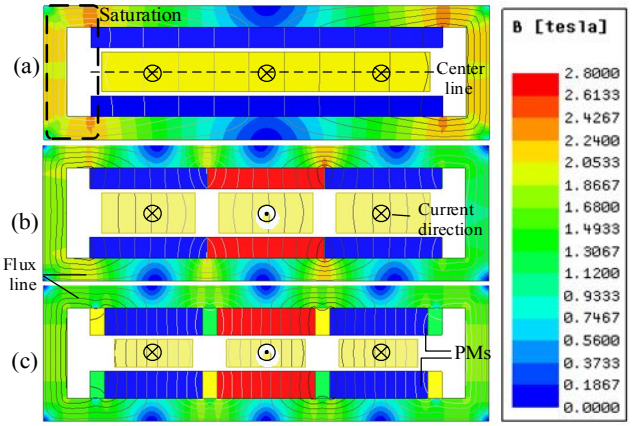



Figure 3. Flux density, flux line and current directions of VCAs. (a) Common structure. (b) Segmented structure. (c) Halbach structure.

As we can see, in Fig. 3-a, the middle part of yoke is wasted as flux density nearly zero; the two side parts are over used as flux density reach the saturation point. The saturation will cause flux density decrease which results in thrust decrease.

The flux density waveform at center line (dash line in Fig. 3) in gap region are compared between these three different structures, as Fig. 4 shows. The red dash line and black dot line belong to common structures whose yoke thickness is 5mm and 10 mm respectively. The blue line belongs to segmented structure and the green line belongs to Halbach structure.

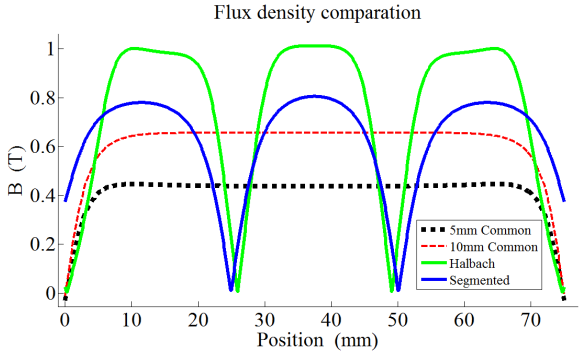



Figure 4. Gap flux density waveform comparison.

Comparing the red and black dash line, flux density increased with yoke thickness increase, because a thicker yoke can relieve saturation as mentioned before. Although, thicken the yoke is a way to improve performance of common structure, it causes the weight increase and makes the device bulky. The blue line and green line possesses stronger flux density, this indicates that segmented structure and Halbach structure can improve flux density by making full use of yoke. Besides, Halbach structure increases flux density further compared to segmented structure, but simply increasing flux density does not guarantee performance improving, this will be studied in part B.

*B. Thrust modeling.*

The armature reaction caused by coil current is ignored as its influence is small. Most literatures use the formula below to model the force that VCA produces.

$$F = NBLI \tag{1}$$

$N$ represents turns of coil, $B$ is average flux density, $I$ is the input current and $L$ is the effective length, it is the length of VCA in vertical paper direction as Fig. 2 shows. However, this equation is inaccurate as the limitation of $N$ is ignored. $N$ is not a free variable, the area that wire should be winded is governed by the flux density distribution as Fig. 5 shows. Conductors in the useless area produce little force but copper loss is still existing. The useful area corresponding to the top part of the flux density waveform, coils should exactly winded in this area. If coils are too wide, there will be a waste of copper with unnecessary copper loss and force ripple; if coils are too narrow, there will be a waste of PMs with unnecessary thrust loss. Therefore, $N$ is determined by the useful area.

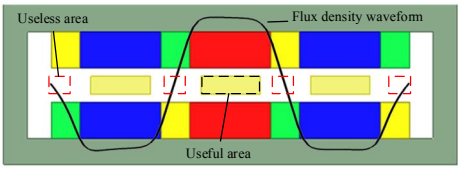



Figure 5. Coil section area with flux density waveform.

Firstly, the accurate thrust model is established in this way. Considering ideal winding, there is no cracks between wires. Considering the force produced by ever conductors, $J$ is current density, $r$ is the wire radius. We have

$$F = \sum_{1}^{N} BLI = LJ \sum_{1}^{N} B\pi r^2 = LJ \iint_A B \,\mathrm{d}x\mathrm{d}y \tag{2}$$

The integral area $A$ is exactly coil cross-section area, notice that it is varying with the coil displacement, it's not the fixed useful area in Fig. 5. Thus thrust at different coil displacement is accurately modeled. In other words, the force ripple is predicted simultaneously.

There is an obvious difference between (1) and (2). For (1) the input is current; for (2) the input should be current density. There are some literatures applied $K_f$ (output force @1A, called as force constant or force sensitivity), to evaluate the output capability of VCA, but according to (2), $K_f$ is influenced by wire radius. If wire radius is not uniformed, this evaluation is prejudiced. There are some literatures mentioned that shrink wire radius will increase $K_f$, force sensitivity, that the resolution is improved, at the price of temperature rise as thin wire will produce more heat. Interestingly, from (2), it can be inferred that the heat production is irrelevant with wire radius.

For profound understanding, to highlight the feature of wire radius, Table 1 is presented. $\rho$ is the conductivity, $l_{cp}$ is the average perimeter of one turn coil and $v$ is the operating velocity of the actuator.

TABLE 1. EXPRESSIONS OF DIFFERENT PROPERTIES

| **Properties** | **Expressions** | **Relationship with *r*** |
|---|---|---|
| Wire radius | $r$ | $=r$ |
| Resistance | $R = \rho \frac{Al_{cp}}{\pi^2 r^4}$ | $\propto r^{-4}$ |
| Force sensitivity | $K_f = \frac{L}{\pi r^2} \iint_A B \mathrm{d}x\mathrm{d}y$ | $\propto r^{-2}$ |
| **Force per current density** | $F/J = L \iint_A B \mathrm{d}x\mathrm{d}y$ | $\propto r^0$ |
| **Force** | $F = LJ \iint_A B \,\mathrm{d}x\mathrm{d}y$ | $\propto r^0$ |
| **Copper loss** | $Q = I^2R = J^2 \rho A l_{cp}$ | $\propto r^0$ |
| **Input Power** | $P = Fv + I^2R$ | $\propto r^0$ |

As we can see, with the same current density, force and copper loss are fixed. Copper loss is the vast majority of heat production which determines temperature rise. That is, with the same force output, shrinking wire radius won't influence heat and temperature rise. Besides, the force output capability of VCA can be demonstrated by force per current density.

It is concluded as

1) For the same output force, copper loss and input power is irrelevant with wire radius.

2) Force per current density is the index of force output capability.

The conclusion above is based on ideal winding, actually, there are cracks between conductors and results in a shrink of $A$. The properties in Table 1, expect $r$, will shrink the same time with $A$. The shrink factor is mainly decided by the processing technic and slightly influence by wire radius. The crack area of three contacted identical circle is always $(2\sqrt{3}-\pi)/2\pi$ of one circle area, this is why $r$ can hardly influence the shrink factor. Therefore, conclusions can generalize to actual winding situation.

The key of VCA design is the integral of flux density, $\iint_A B\mathrm{d}x\mathrm{d}y$. Simply improving flux density does not guarantee the performance improving.

Secondly, analytically model of the flux density is developed. As Fig. 6 shows, the parameters are specifically labeled. Flux density of $x$ component is ignored in this paper, it is small and produce force in $y$ direction.

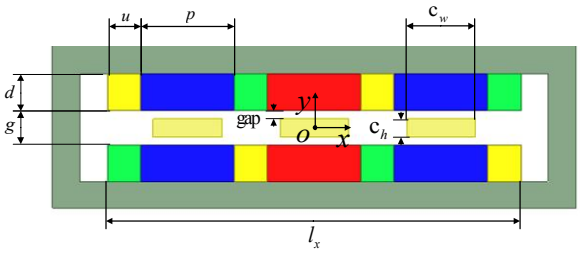



Figure 6. Halbach structure VCA labeled with parameter names and coordinate.

$d$ is the thickness of PMs, $g$ is the thickness of air region, $c_w$ and $c_h$ are coil cross-section width and height respectively.

Analytical method is applied to solve the magneto-static Maxwell equation via calculating magnetic vector potential. The magneto-static Maxwell equation

$$\nabla \times \vec{B} = -\nabla^2 \vec{A} \tag{3}$$

Where $\vec{A}$ is the magnetic vector potential. The process of solving the equation is omitted. The flux density of $y$ component in gap region is

$$B_y = \sum_{n=1}^{\infty} C_n' k_n \cosh(k_n y)\cos(k_n x) \tag{4}$$

For clarity, $C_n' = C_n'(d, g, p, l_x)$ and $k_n$, is presented in appendix. Substituting (4) into (2) the thrust model is written as

$$F = LJ \sum_{n=1}^{\infty} \iint_A C_n' k_n \cosh(k_n y)\cos(k_n x)\,dx dy \tag{5}$$

### C. Flexure-based membrane design

The design objectives of flexure-based bearing have large stroke, constant stiffness and supporting (off-axis stiffness), i.e., in millimeters stroke keep the stiffness almost invariant while the off-axis stiffness is high enough to support the moving coils. A flexure-based membrane is designed. The flexure-based membrane formed by four same pieces of beam-based flexure units, is jointed together as Fig. 7 shows. One VCA need a pair of membranes arranged both sides to support coils, the two membranes comprise double parallelogram flexure mechanism. This mechanism prevents the parasitic motion along $y$-axis and ensures the homogenization of the air gap. The upper and lower edge are fixed to the base of the VCA, while the middle part is fixed to the coil supporter.

The membrane accumulates small deformation produced by multiple beams segments connected in 'S' shape. In this example, each beam-based flexure unit can be equivalent to four bend segments whose length and width are $l_b$ and $w_b$, two short torsion segments whose length and width are $l_{t_1}$ and $w_t$ and three long torsion segments whose length and width are $l_{t_2}$ and $w_t$, as Fig. 7-b shows .

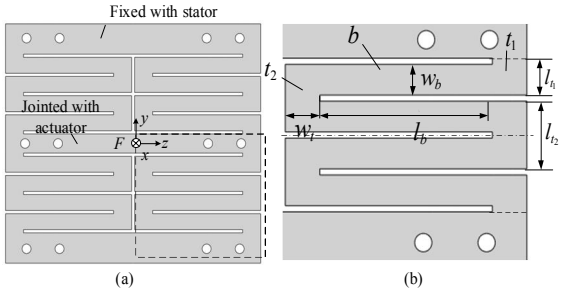



Figure 7. (a) Flexure-based membrane. (b) Beam-based flexure unit.

Based on the principle of equivalence, bend and torsion segments are equivalent to bend springs and torsional springs respectively. The displacement equivalent stiffness of the whole flexure-based membrane is deduced by the principle of series-parallel stiffness of springs. The equivalent translation stiffness of a pair of flexure-based membranes is

$$k_{eq,\text{trans}} = \frac{8}{2/k_{t1} + 3/k_{t2} + 4/k_b} \tag{6}$$

$k_t, k_b$ are the stiffness of twist segment and bend segment respectively. $k_{t1}, k_{t2}$, are to distinguish the short torsional segment and long torsional segment.

Equations (7) and (8) are obtained from Chen[15] and the semi-analytical model[16] respectively.

$$k_t = \frac{G t w_t^2}{3.5 l_t^2 (1 + w_t^2 / t^2)} \tag{7}$$

$$k_b = \frac{2EI\theta}{l_b^2 \eta (L+S)\sin\theta \sin(\pi/2 - \theta)} \tag{8}$$

$G$ and $t$ denote shear modulus and thickness of flexure respectively. $E$ and $I$ represent the Young's Modulus and second moment of area respectively, $\eta$ and $S$ is presented in appendix where $L = 0$ . Substituting (7) and (8) into (6), the value of equivalent translation stiffness $k_{eq,\text{trans}}$ can be obtained.

## III. Verification and Experiments

The FEA software, ANSYS, is used to verify the design primarily, then it is experimentally verified. Manual positioning stage carrying with the ATI's force/torque sensor is used to push the device, while the laser interferometer system (KEYSIGHT) records the displacement of actuator, as Fig. 8 shows. When VCA is power-off, the force-displacement relationship of flexure-based membranes is measured. Powered by MOTECH LPS 305 DC power supply, the resultant force produced by VCA and flexure-based membranes is measured, minus the flexure-based membranes' force measured before, the VCA force output is obtained.

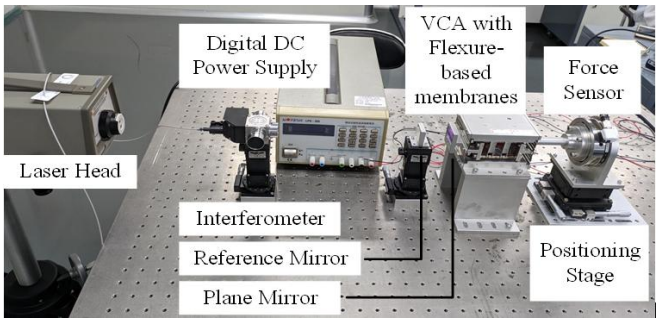



Figure 8. Experimental setup.

### A. *The Stiffness of Flexure-based Membrane*

The relationship of force-displacement is given as

$$F = k_{eq,trans}\delta \tag{9}$$

Spring steel 65Si2Mn is selected as the material of flexure-based membranes, $k_{eq,trans} \approx 4641$ N/m by (8). The theoretical calculation, the FEA result and experiment results are presented in Fig. 9. Besides, *y*-axis stiffness of $4.46\times10^5$ N/m is obtained by FEA and it is enough to support the coil.

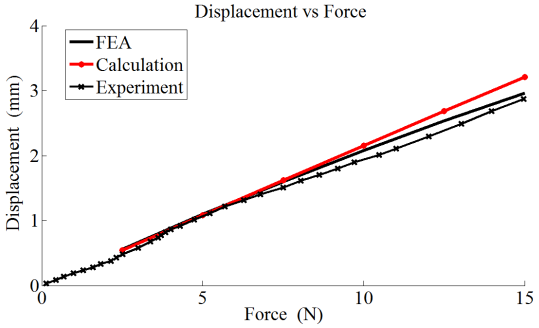



Figure 9. Relationship between displacement and force

The flexure-based membranes equivalent model is in agreement with FEA result within 10 N. Due to processing error, the experimental result shows a higher stiffness about 5000 N/m, it's 8% higher than simulation. Although the stiffness is higher, the relationship between displacement and force is nearly linear.

### B. *Optimization of VCA and thrust experiment*

The ANSYS verification of thrust model is presented in Fig. 10.

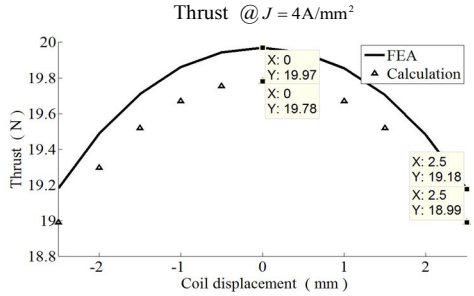



Figure 10. Thrust verification for 5 mm stroke.

Then the genetic algorithm is applied to optimize parameters. The reason that choose GA is as follows

The expression is complicated. Here, we have two objectives, force and force ripple. Force ripple is the force difference between center position and stroke limitation position, in percentage form. A multi-objects and multi-variables problem is to be solved. The Non-domination Sorting Genetic Algorithms - Ⅱ (NSGA-Ⅱ) was implemented to search the optimal parameters. It has advantages with fast convergence and good global optimizing ability.

The volume of the VCA is fixed with two objectives, the thrust and the force ripple, the variables are [ $d$ $p$ $c_w$ ], in millimeter. The boundaries are [2 10 10] to [9 25 24]. The population size is 100 with 150 generations iteration.

The result of NSGA-Ⅱ is presented in Fig. 11. As we can see, result converged after 150 generation iteration. The points encircled by brown dash line, belongs to segmented structure, although the thrust is high, the force ripple is high which will hamper the control performance. The orange one belongs to corresponding to Halbach structure.

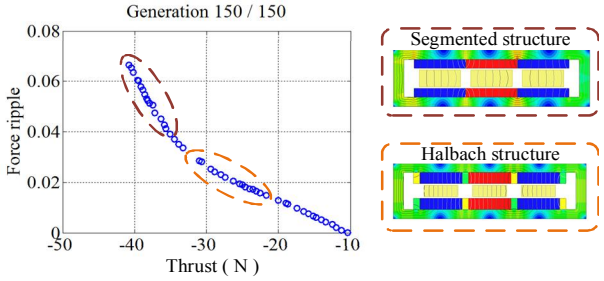



Figure 11. GA result with corresponding structure.

Giving consideration to achieve high linearity with low heat production (small coil cross-section area), 2% force ripple with about 25 N thrust is chosen. Correspondingly the parameters are [6 21 13.5]. As we can see, it's a high price for pursing high linearity with low heat production, the thrust almost reduce a half compared to the highest thrust.

The experimental force output of VCA is presented in Fig. 12.

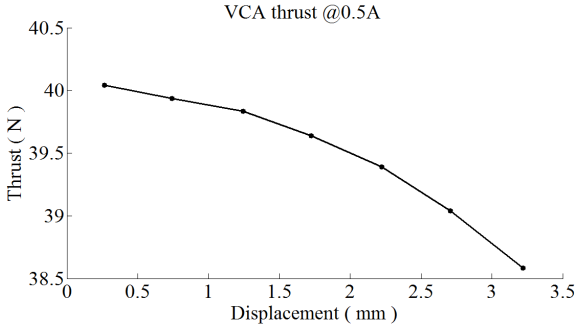



Figure 12. Experimental VCA thrust at 0.5A.

It is in actual winding situation, the experiential estimation thrust is 45N. The experimental force output is

lower than the experiential estimation due to processing loss i.e. the coil is not well winded. The force ripple is about 2% and well agree with the established model. Because the force ripple is decided by the shape of coil, lightly loosen coil won't influence force ripple.

## IV. CONCLUSION

The Halbach VCA along with its flexure-based membrane is designed to deliver millimeters stroke. Turns of coil, *N*, is proved to be determined by the flux density distribution. The accurate VCA thrust model is established and verified, based on the model, it is inferred that wire radius is irrelevant with copper loss and input power, the force output capability of VCA can be evaluated by force per current density. Via GA, the optimal parameters are determined when volume is fixed. The device is fabricated, assembled and experimented. Experimental results show the correctness of established models and feasibility of the design.

## APPENDIX

$$C_n' = -\frac{\mu_0\mu_r(b_n - b_n\cosh(dk_n) + a_n\sinh(dk_n))}{k_n(\cosh(dk_n)\sinh(\frac{gk_n}{2}) + \mu_r\cosh(\frac{gk_n}{2})\sinh(dk_n))}$$

$$b_n = \frac{2B_r}{\mu_0 k_n l}(\cos(k_n(\frac{3}{2}p+2v))-\cos(k_n(\frac{1}{2}p+v))+\cos(\frac{k_n}{2}p))-\cos(k_n(\frac{3}{2}p+v)))$$

$$a_n = \frac{2B_r}{\mu_0 k_n l}(\sin(k_n(\frac{3}{2}p+v))-\sin(\frac{k_n}{2}p)-\sin(k_n(\frac{p}{2}+v)))$$

$$k_n = n\pi / l$$

$$\eta = 1/(2\varpi)$$

$$\varpi = 1-\theta^2/3!+\theta^4/5!$$

$$S = \left(\frac{(l_b/2)\sqrt{1.8}+L}{l_b/2+L}\right)\eta\,(l_b/2)$$

$$I = (t^3 w_b)/12$$

## ACKNOWLEDGEMENT

The authors acknowledge funding provided by the NSFC Zhejiang Joint Fund for the Integration of Industrialization and Informatizaton (U1609206), the Zhejiang Basic Public Welfare Research Project (LGG18E070007) and Major Project and Key S&T Program of Ningbo (2017B10014).

## REFERENCE

[1] Shorya Awtar, Gaurav Parmar. "Physical and Control System Design Challenges in Large Range Nanopositioning". IFAC Proceedings Volumes, 43(18): 152-159, 2010.

[2] Shorya Awtar, Gaurav Parmar. "Design of a Large Range XY Nanopositioning System". Journal of Mechanisms and Robotics, 5(2): 21008, 2013.

[3] T J Teo, G Yang, I M Chen. "A Flexure-based Electromagnetic Nanopositioning Actuator with Predictable and Re-configurable Open-loop Positioning Resolution". Precision Engineering-Journal of the International Societies for Precision Engineering and Nanotechnology, 40: 249-260, 2015.

[4] Viet Phuong Bui, Guilin Yang, I-Ming Chen, Tat Joo Teo. "Millimeters Stroke Nanopositioning Actuator With High Positioning and Thermal Stability". IEEE/ASME TRANSACTIONS ON MECHATRONICS, VOL. 20(NO. 6): 2813-2835, 2015.

[5] L Dong, J Chen, C Zhang, et al. "A Novel Voice Coil Motor Used in Nano-positioning Device", 2015 18th International Conference on Electrical Machines and Systems. 1997-2002, 25.

[6] Steven M. Lund, Klaus Halbach. "Iron-free Permanent Magnet Systems for Charged Particle Beam Optics". Fusion Engineering and Design, 32: 401-415, 1996.

[7] K Halbach. "Perturbation Effects in Segmented Rare Earth Cobalt Multipole Magnets". Nuclear Instruments and Methods in Physics Research, 198(2): 213-215, 1982.

[8] Moon G. Lee, Young Man Choi, Sung Q. Lee. "Design of high precision linear stage with double-sided multi-segmented trapezoidal magnet array and its compensations for force ripples". Mechatronics, 16(6): 331-340, 2006.

[9] Moon G. Lee, Sung Q. Lee, Dae-Gab Gweon. "Analysis of Halbach magnet array and its application to linear motor". Mechatronics, 14(1): 115-128, 2004.

[10]Meessen K.J., Paulides . "Analysis of 3-D Effects in Segmented Cylindrical Quasi-Halbach Magnet Arrays". IEEE Transactions on Magnetics, 47(4): 727-733, 2011.

[11] Sun Jinji, Ren Yuan, Fang Jiancheng. "Passive Axial Magnetic Bearing with Halbach Magnetized Srray in Magnetically Suspended Control Moment Gyro Spplication". Journal of Magnetism and Magnetic Materials, 323(15): 2103-2107, 2011.

[12] Meessen, K.J. ,Gysen . "Halbach Permanent Magnet Shape Selection for Slotless Tubular Actuators". IEEE Transactions on Magnetics, 4(11): 4305-4308, 2008.

[13]Qingsong Xu. "New Flexure Parallel-Kinematic Micropositioning System With Large Workspace". IEEE TRANSACTIONS ON ROBOTICS, 28(2): 478-491, 2012.

[14] Gaurav Parmar, Kira Barton, Shorya Awtar. "Large dynamic range nanopositioning using iterative learning control". Precision Engineering, 38(1): 48-56, 2014.

[15] Guimin Chen , Larry L. Howell. "Two general solutions of torsional compliance for variable rectangular cross-section hinges in compliant mechanisms". Precision Engineering, 33(3): 268-274, 2008.

[16] Teo,Tat Joo, I M Chen . "A generic approximation model for analyzing large nonlinear deflection of beam-based flexure joints". Precision Engineering, 34(3): 607-618, 2010.